DEVELOPMENT OF A STEAM GENERATOR TUBE INSPECTION ROBOT WITH A SUPPORTING LEG

HOCHEOL SHIN*, KYUNG-MIN JEONG, SEUNGHO JUNG and SEUNGHO KIM
Nuclear Robotics Laboratory, Korea Atomic Energy Research Institute
1045 Daedeokdaero, Yuseong, Deajeon 305-353, Korea
*Corresponding author. E-mail : smarthc@ kaeri.re.kr

Received November 27, 2007
Accepted for Publication September 16, 2008

This paper presents details on a tube inspection robotic system and a positioning method of the robot for a steam generator (SG) in nuclear power plants (NPPs). The robotic system is separated into three parts for easy handling, which reduces the radiation exposure during installation. The system has a supporting leg to increase the rigidity of the robot base. Since there are several thousands of tubes to be inspected inside a SG, it is very important to position the tool of the robot at the right tubes even if the robot base is positioned inaccurately during the installation. In order to obtain absolute accuracy of a position, the robot kinematics was mathematically modeled with the modified DH(Denavit-Hartenberg) model and calibrated on site using tube holes as calibration points. To tune the PID gains of a commercial motor driver systematically, the time delay control (TDC) based gain tuning method was adopted. To verify the performance of the robotic system, experiments on a Framatome 51B Model type SG mockup were undertaken.

KEYWORDS : Steam Generator Tube Inspection Robot, Robot Calibration, Modified DH Model, Time Delay Control

1. INTRODUCTION

A SG of NPPs is a heat exchanger which is internally in contact with the primary coolant and externally in contact with the secondary coolant. The secondary coolant is vaporized. There are several thousands of heat exchange tubes of which the thickness is about 1mm. The integrity of the relatively thin tubing can therefore influence the degree of radioactive contamination appearing in the secondary side in the event of tube leaks. For this reason, inspection and maintenance of these SG tubes is very important from the viewpoint of the integrity of the NPPs. Eddy current testing (ECT), one of nondestructive evaluation (NDE) techniques, is usually used to evaluate the integrity of the tube pressure boundary. Practically all tasks have to be performed remotely because the chamber is a high radiation area. A robotic arm with a precise positioning capability shall be entered into the chamber through a manway which is about 40cm in diameter [1-3].

Numerous research and development works on automatic inspection and automatic repair of SG tubes have been performed until now [5-11]. There are two types of SG tube inspection robots: the tube-walking type and the manipulator type. Although tube walking type robots such as Pegasys [5] and MR-III [6] are lightweight and capable of precise positioning, there is a possibility of the manipulator falling off the tube sheet. To avoid interior damage in the SG chamber resulting from the robot's falling from the tube sheet, great care is required. Because the installation of this type of robots is somewhat difficult, the radiation exposure will be increased during installation.

Manipulator type robots can be fixed on the tube sheet or the manway flange. ROSA III [7] and FLEXIVERA [8] use the tube sheet to fix themselves. In this case, the robot base can be positioned accurately. But it is difficult for human workers to fix the robots on the tube sheet, which increases installation time to increase the radiation exposure. In addition, the robot base must be moved to other tubes in order to inspect the tubes used for fixing the robot. Some of these are designed to maintain the rigidity, which guarantees the accuracy but makes the robots so heavy that it is difficult to handle them.

To install SM23 [9], a fixture that consists of an entering/exiting rail guide and a pose adjusting device is fixed on the manway flange and then the manipulator slides into the end of the fixture. Thus, it is easy to handle and to install it, resulting in reduced radiation exposure. However, the manipulator and the entering/exiting device are so lightweight and long that they are deflected a lot. Such deflections and the inaccurately positioned robot

base during installation result in large positioning errors for the tool during inspection. Therefore, the robot needs on-site calibration to be able to precisely insert an ECT probe into the target tube among the thousands of tubes. There have been research works on calibration of a SG tube inspection robot with a machine vision system [10-11]. However it also requires initial calibration of the robot.

In this research, a manipulator type robot fixed on the manway was developed in order to reduce the radiation exposure to human workers. To reduce the effect of deflection, the robotic system was designed to have a supporting leg under the manipulator base. To obtain good control performance systematically, this paper provides details of calibration, main control program with 3D graphic GUI, and motor driver's gain tuning method. To verify the performance of the developed robotic system, experiments, on a Framatome 51B Model type SG mockup, were undertaken and the results are provided in chapter 4.

2. ROBOT SYSTEM

2.1 Robot Design

The proposed robot was designed to be mounted on the manway for quick installation, so that workers receive lower doses of radiation as described previously. The developed robot system in a SG chamber is shown in Fig. 1. For easy conveyance and installation, the robot is made up of three separable parts: a manipulator base pose adjusting device, a water-chamber entering/exiting device, and a manipulator.

Fig. 2 shows the installing procedure of the robot. Fig. 2(a) shows the manway flange on which the manipulator base pose adjusting device is mounted. The manipulator base pose adjusting device has swing and roll axes to adjust the position and level of the manipulator base. Fig. 2(b) shows the manipulator entering/exiting device, which is fixed to the base pose adjusting device. The manipulator

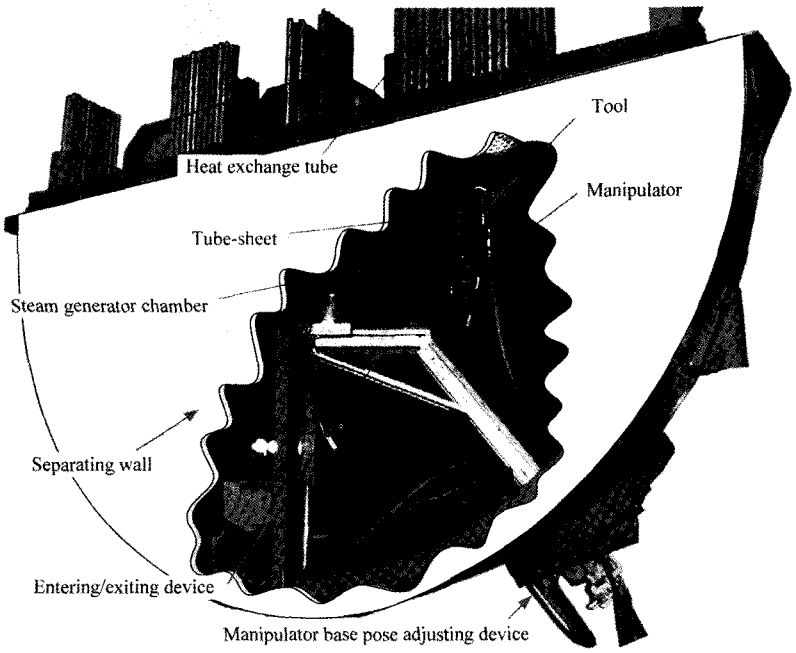

Fig. 1. Steam Generator Heat Exchanging Tube Inspection/Maintenance Robot

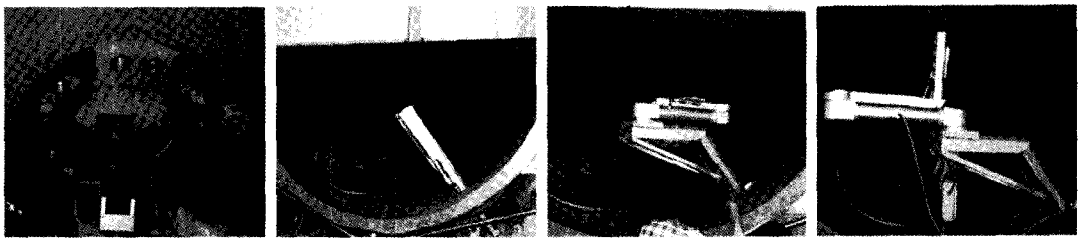

(a) (b) (c) (d)

Fig. 2. Installing Procedure of the Robot

slides along the rail of the device and then the manipulator is clamped at the top of the device. Fig. 2(c) shows a leveling mechanism of the device on which the manipulator is mounted. Fig. 2(d) shows a supporting leg, which improves the rigidity of the system, so that the overall accuracy is increased and the vibration level is reduced when the manipulator is moving. The manipulator has two links that rotate on the horizontal plane, and a mast that moves linearly in vertical direction. The full length of the manipulator is about 1.5 m. An inspection tool is connected to the mast. The manipulator positions the tool on the target tube.

2.2 Robot Control System

After installation, the robot is operated at a distance of 100 m from the SG chamber for the safety of its operator. The control system as shown in Fig. 3 consists of three parts: a controller box, a main control computer and a video/audio system.

The robotic system is installed in the SG chamber. The controller box is placed near the SG. For easy operation, an industrial PC with the Windows NT Operating System is used as the main control computer. The main control computer is located in a vehicle or a control room 100 m away from the SG, and communicates with the motion controller in the controller box and an ECT data acquisition system through LAN cables. A robot operator communicates with a worker at the site through the audio system, and monitors the situation in and around the SG chamber through the video system.

To carry out the inspection works of the SG tubes, a main control program was developed. The GUI of the program is based on real time 3D graphics. The control program consists of a setup mode, a trunk setting mode, a robot setting mode, a calibration and manual mode, and a scheduling and inspection mode. The trunk means the entering/exiting device. SG type data, robot type data and motion controller type data are provided as a text file. The program commands the robot through Ethernet. Fig. 4 shows the structure of the control program and Fig. 5 shows the GUI of the control program.

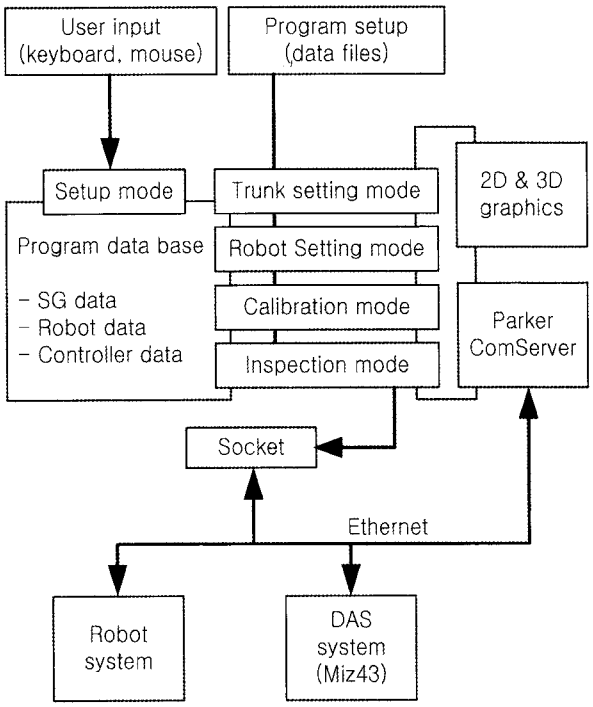

Fig. 4. Structure of the Control Program

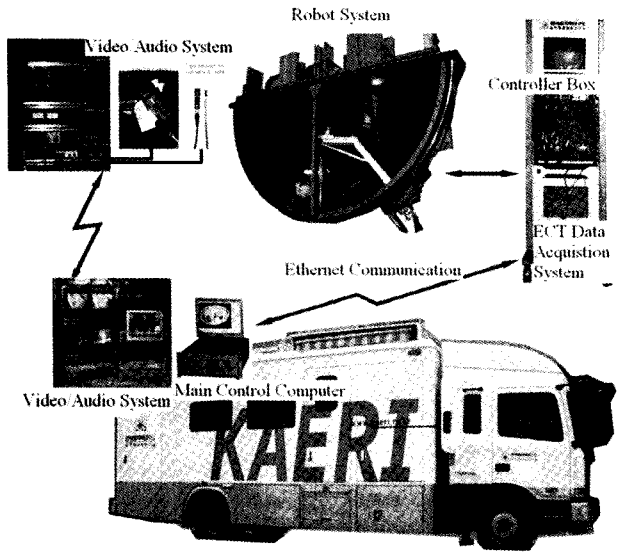

Fig. 3. Remote Robot Control System

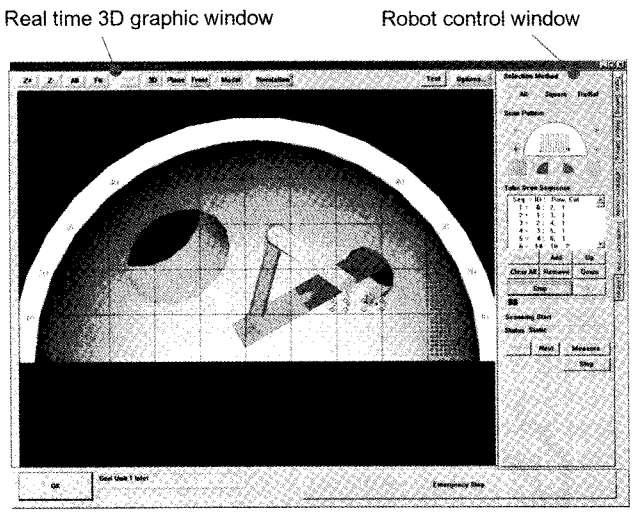

Fig. 5. GUI of the Control Program

3. TOOL POSITIONING

3.1 Manipulator Calibration

To insert the ECT probe into a SG tube with a small diameter of about 20 mm, the inspection tool should be positioned on the target tube accurately. Joint angles of the manipulator can be obtained for a desired tool position through a kinematic model. However, positioning errors exist since the manipulator base point changes during installation and deviations occur between the kinematic model used in the controller and in the actual arm geometry. Besides, the manipulator is deflected considerably due to its long length. To reduce these errors, the kinematic model of the manipulator should be calibrated whenever it is installed. If the positioning errors increase to a certain value, the manipulator needs more calibration, which is a tedious task.

The DH (Denavit-Hartenberg) model is popular for modeling manipulator kinematics; however, there are some limitations in using this model for a calibration procedure. The most important limitation of the DH formalism is the treatment of the consecutive revolute joints with nearly parallel axes, since there are convergence problems in the parameter identification routines [12].

The 1st joint and the 2nd joint of the proposed manipulator are revolute joints with parallel axes as shown in Fig. 6. To solve this problem, a modified DH model proposed by Hayati and Mirmirani [13] was used for the consecutive parallel axes. Fig. 6 shows the coordinate frames. The origin of the world coordinate ($X_wY_wZ_w$) was defined by the mid point of the first row of the SG tubes and the XZ plane of the world coordinate was defined by the tube sheet plane. The coordinate $X_0Y_0Z_0$ is fixed on the manipulator base and the coordinate $X_iY_iZ_i$ is fixed on the i-th link, respectively.

The homogeneous transformation matrix of the modified DH model for adjacent frames, i and i-1, is

$$
{}^{i-1}\mathbf{A}_i = \mathbf{R}(z,\theta_i)\mathbf{T}(r_i,0,0)\mathbf{R}(x,\alpha_i)\mathbf{R}(y,\beta_i)
$$

$$
= \begin{bmatrix} -s\alpha_i s\beta_i s\theta_i + c\beta_i c\theta_i & -c\alpha_i s\theta_i & s\alpha_i c\beta_i s\theta_i + s\beta_i c\theta_i & r_i c\theta_i \\ s\alpha_i s\beta_i c\theta_i + c\beta_i s\theta_i & c\alpha_i c\theta_i & -s\alpha_i c\beta_i c\theta_i + s\beta_i s\theta_i & r_i s\theta_i \\ -c\alpha_i s\beta_i & s\alpha_i & c\alpha_i c\beta_i & 0 \\ 0 & 0 & 0 & 1 \end{bmatrix} \tag{1}
$$

where $\mathbf{R}$ is the rotation matrix, $\mathbf{T}$ is the translation matrix, $s\theta=\sin\theta$, $c\theta=\cos\theta$, α_i and β_i are the rotations about the indicated axes, θ_i is the joint variable and r_i is the length of the consecutive parallel axes. Fig. 7 shows the modified DH model parameters.

The transformation from the world coordinate frame W to the coordinate frame 3 is

$$
\mathbf{T}_3 = {}^{W}\mathbf{A}_0\,{}^{0}\mathbf{A}_1\,{}^{1}\mathbf{A}_2\,{}^{2}\mathbf{A}_3 . \tag{2}
$$

Since the coordinate frames 0, 1 and 2 have nearly parallel joint axes, which may have convergence problems as explained above, the modified DH model is adapted to ${}^{0}\mathbf{A}_1$ and ${}^{1}\mathbf{A}_2$. And the DH model is used for the homogeneous transformation matrixes ${}^{W}\mathbf{A}_0$ and ${}^{2}\mathbf{A}_3$ as follows.

$$
{}^{W}\mathbf{A}_0 = \mathbf{R}(z,\theta_0)\mathbf{T}(0,0,d_0)\mathbf{T}(a_0,0,0)\mathbf{R}(x,\alpha_0) \tag{3}
$$

$$
{}^{2}\mathbf{A}_3 = \mathbf{R}(z,0)\mathbf{T}(0,0,d_3)\mathbf{T}(0,0,0)\mathbf{R}(x,0) \tag{4}
$$

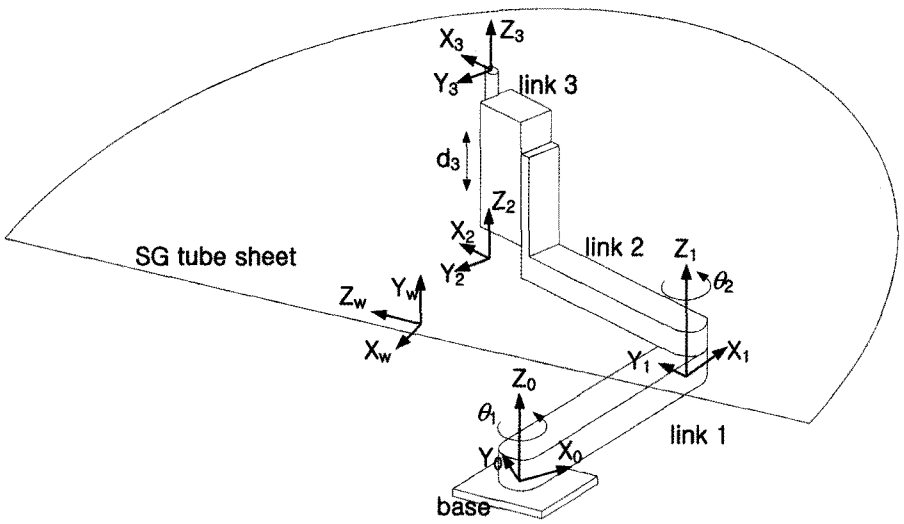

Fig. 6. Coordinate Frame Assignment

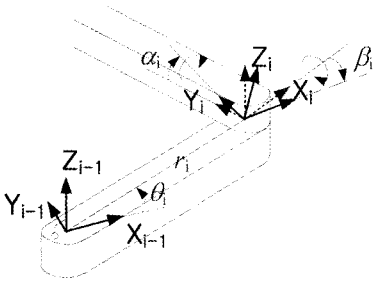

Fig. 7. Modified DH Model Parameter

From now, let the homogeneous transformation matrix ${}^{i-1}\mathbf{A}_i$ be $\mathbf{A}_i$. And let ${}^{W}\mathbf{A}_0$ be $\mathbf{A}_0$. The link kinematic error model is expressed by a nominal value $\mathbf{A}_{iN}$ and an error $d\mathbf{A}_{iN}$ as follows.

$$\mathbf{A}_i = \mathbf{A}_{iN} + d\mathbf{A}_{iN}.$$
$$d\mathbf{A}_{iN} = \sum_{j=1}^{Pi} \frac{\partial \mathbf{A}_{iN}}{\partial k_{ij}} \Delta k_{ij}, \quad i = 0, 1, 2, 3. \tag{5}$$

Here, k_{ij} is the j-th parameter of $\mathbf{A}_i$ and P_i is the number of parameters of $\mathbf{A}_i$.

The manipulator kinematic error model is

$$\mathbf{T}_3 = \mathbf{T}_{3N} + d\mathbf{T}_{3N} = \prod_{i=0}^{3} (\mathbf{A}_{iN} + d\mathbf{A}_{iN}). \tag{6}$$

By expanding Equation (6) and ignoring the second-order products, we obtain

$$d\mathbf{T}_{3N} = \mathbf{T}_{3N} \delta\mathbf{T}_{3N},$$
$$\delta\mathbf{T}_{3N} = \sum_{i=0}^{3} \mathbf{U}_{i+1}^{-1} \delta\mathbf{A}_i \mathbf{U}_{i+1}. \tag{7}$$

Here, $\mathbf{U}_n = \prod_{i=0}^{n} \mathbf{A}_{iN}$. And the error of the transformation, $\delta\mathbf{T}_{3N}$, can be defined as the small displacement of dx, dy and dz, and the small rotations δx, δy and δz. It can be shown that

$$\delta\mathbf{T}_{3N} = \begin{bmatrix} 0 & -\delta z & \delta y & dx \\ \delta z & 0 & -\delta x & dy \\ -\delta y & \delta x & 0 & dz \\ 0 & 0 & 0 & 0 \end{bmatrix}. \tag{8}$$

Because only the SG tube holes can be used as calibration points, we can only obtain the position error of the tool frame for a calibration point **e**. After some manipulation **e** can be obtained using a Jacobian(**J**) of a 4×13 matrix.

$$\mathbf{e} = d\mathbf{T}_{3N}\mathbf{M} = \mathbf{T}_{3N}\delta\mathbf{T}_{3N}\mathbf{M} = \mathbf{T}_{3N}\mathbf{J}\delta\mathbf{k}. \tag{9}$$

Here, $\mathbf{M}=[0\ 0\ 0\ 1]^T$ and $\delta\mathbf{k}$ is the 13×1 column vector of the kinematic link parameter errors. If the position error vectors and the Jacobian matrixes are augmented for all calibration points, $\delta\mathbf{k}$ is obtained using a pseudo inverse as follows.

$$\delta\mathbf{k} = \left((\mathbf{J}_A^T\mathbf{J}_A)^{-1}\mathbf{J}_A^T\right)\left[\mathbf{T}_{3N}^{-1}\mathbf{e}\right]_A. \tag{10}$$

Here, $\mathbf{J}_A$ is an augmented Jacobian matrix.

3.2 Control Gain Tuning

The manipulator is controlled by a PID controller. To tune the PID gains of a commercial motor driver systematically, a TDC-based gain tuning method was adopted [14, 15]. TDC has an inherently compact and robust property. Therefore, the tuning procedure of the PID control can be simple and straightforward. Also the TDC-based gain tuning method provides robustness for the PID control.

The control input of a TDC is given by

$$\tau(t) = \tau(t-\lambda) + \overline{M}\left(-\ddot{\theta}(t-\lambda) + \ddot{\theta}_d(t) + K_D\dot{e}(t) + K_P e(t)\right), \tag{11}$$

where λ is the time delay and $\overline{M}$, K_D and K_P are the parameters of TDC. $\overline{M}$ determines the stability and performance of the TDC. K_D and K_P are determined from an error dynamics which has a desired natural frequency and a damping ratio[15].

By approximating the angular velocity and acceleration with the backward difference method, the control input can be expressed as follows.

$$\tau(k) = \tau(k-1) + \overline{M}\left[\ddot{\theta}_d(k) - \frac{1}{L^2}(\theta(k) - 2\theta(k-1) + \theta(k-2)) + K_D\left(\dot{\theta}_d(k) - \frac{1}{L}(\theta(k) - \theta(k-1))\right) + K_P(\theta_d(k) - \theta(k))\right], \tag{12}$$

where, L is the sampling time of the control system.

Fig. 8 shows a block diagram of the PID controller

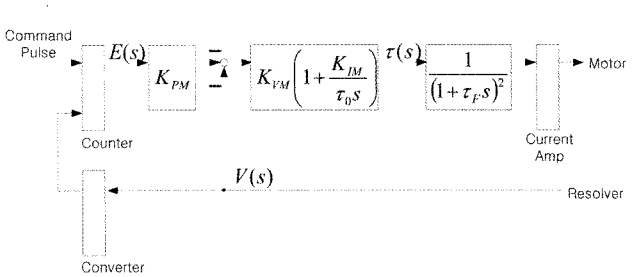

Fig. 8. Block Diagram of the PID Controller of the Driver

imbedded in the Tamagawa motor drivers. From the block diagram, the input torque of the motors can be calculated as follows.

$$\tau(s) = -(K_{PM}E(s) + V(s))K_{VM}\left(1 + \frac{K_{IM}}{\tau_0 s}\right)$$
$$= -K_{VM}\left(K_{PM} + \frac{K_{IM}}{\tau_0} + \frac{K_{IM}K_{PM}}{\tau_0}\frac{1}{s} + s\right)E(s), \quad (13)$$

where, $E(s) = \mathcal{L}(e(t)), V(s) = \mathcal{L}(\dot{e}(t))$ and τ_F is the time constant of the low pass filter. In order to implement a PID controller, τ_F is set to zero.

Through the inverse Laplace transform with zero initial conditions followed by the backward difference method, the input torque is expressed as follows.

$$\tau(k) = \tau(k-1) + LK_{VM}\left[\left(\ddot{\theta}_d(k) - \frac{1}{L^2}(\theta(k) - 2\theta(k-1) + \theta(k-2))\right)\right.$$
$$\left. + \left(K_{PM} + \frac{K_{IM}}{\tau_0}\right)\left(\dot{\theta}_d(k) - \frac{1}{L}(\theta(k) - \theta(k-1))\right) + \frac{K_{PM}K_{IM}}{\tau_0}(\theta_d(k) - \theta(k-1))\right]. \quad (14)$$

The PID control gains are calculated from Eq. (12) and (14) as follows.

$$K_{PM} = \frac{K_D \pm \sqrt{K_D^2 - 4K_P}}{2}, \quad K_{IM} = \frac{\tau_0 K_P}{K_{PM}}, K_{VM} = \frac{\overline{M}}{L}. \quad (15)$$

More details can be found in references [15] and [16].

4. EXPERIMENTS

To demonstrate the effectiveness of the developed robotic system, experiments were undertaken in the Framatome 51B Model type SG mockup of which the inner diameter is about 3.2 m. It has 3,330 tubes arrayed in a square pattern of 94 columns and 46 rows with a pitch of 32.51 mm (1.28"). The tube diameter is 19.05 mm (3/4").

4.1 Manipulator Calibration Result

Table 1 shows the nominal values of the kinematic parameters of the developed manipulator. Type 1 means the transformation of the DH model and type 2 that of the modified DH model.

The calibration points are selected by considering a positioning error reduction for the whole working area and easy identification of their location. Eight tube holes are used as calibration points. Half of the holes are located in the 1st quadrant, and the other half of the holes are located in the 2nd quadrant. Table 2 shows the selected calibration points.

To measure the global coordinate data of the calibration points, an operator observes the tool tip through the camera mounted on the tool, and moves the manipulator to place the tool tip at the tubes selected as the calibration points. After the tool has been positioned at all the calibration points, the calibrated kinematic link parameters are obtained through Eq. (10).

Table 3 shows the coordinate values for the calibration points. It is noted that the mean of the errors is about 1 mm and the manipulator can be positioned at every tube hole without further calibration.

Fig. 9 shows the pictures when the tool tip was positioned manually to obtain the global coordinate data

Table 1. Nominal Kinematic Parameters of the Manipulator

Trans.	Type	θ	d	a	α
W→0	1	180°	0.01m	0.15m	90°
0→1	2	0°	0°(ß)	0.69m	0°
1→2	2	-180°	-0.1°(ß)	0.84m	0°
2→3	1	0°	-0.001m	0m	0°

Table 2. Calibration Points on the SG Tube Sheet

No.	1	2	3	4	5	6	7	8
Row	46	40	30	6	46	40	30	6
Column	41	25	13	1	54	70	82	94

Table 3. Coordinate Values for the Calibration Points (m)

Pt.	Actual values			Calculated values after calibration		
	x_w	y_w	z_w	x_w	y_w	z_w
1	-1.4630	0	-0.2113	-1.4635	0.0006	-0.2115
2	-1.2680	0	-0.7315	-1.2677	-0.0004	-0.7332
3	-0.9428	0	-1.1217	-0.9423	-0.0005	-1.1215
4	-0.1626	0	-1.5118	-0.1644	0.0004	-1.5098
5	-1.4630	0	0.2113	-1.4632	-0.0005	0.2102
6	-1.2680	0	0.7315	-1.2676	0.0008	0.7304
7	-0.9428	0	1.1217	-0.9432	-0.0004	1.1220
8	-0.1626	0	1.5118	-0.1610	-0.0001	1.5135

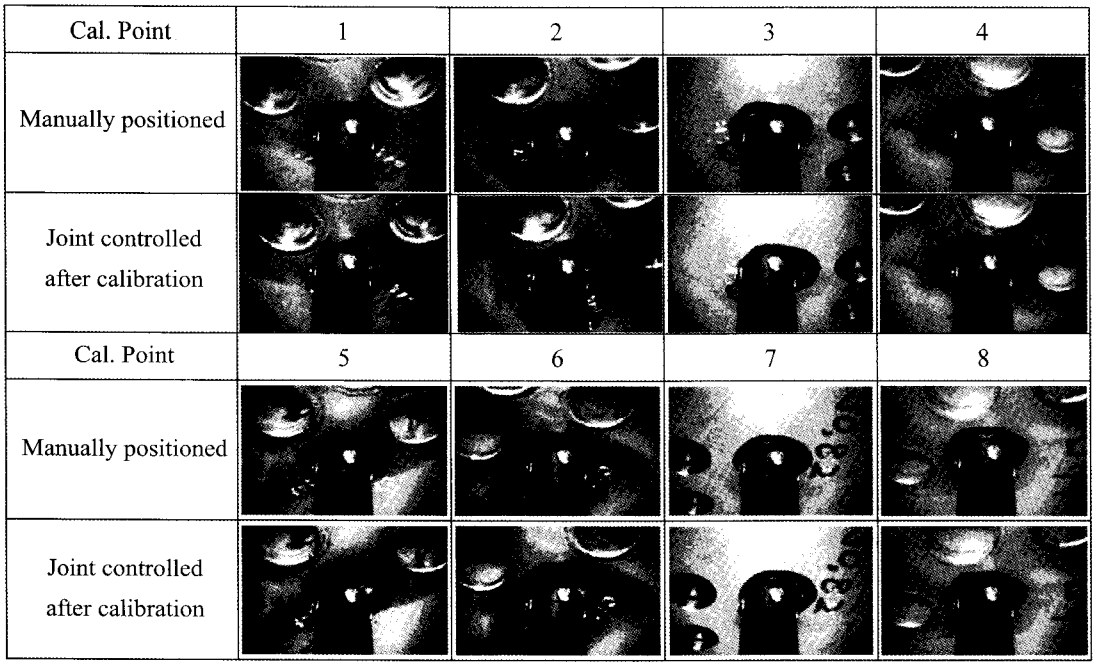

Fig. 9. Calibration Results for the Calibration Points

of the calibration points and when it was positioned again with the joint angles calculated from the calibrated kinematic model for all the calibration points.

Although there are slight deviations between the tube holes and the tool tip, these errors are acceptable. Because the ECT probe has a cone-shaped head and a flexible tail, it can be inserted into the tubes when the error is less than half of the diameter of the tube. If the error is less than a third of the diameter of the tube, then the probe can be inserted smoothly.

Table 4 shows the calibrated kinematic parameters of the manipulator and Fig. 10 shows the resulting coordinate frames, which are nearly all placed in one plane of the tube sheet.

It is noted that the differences between the nominal values and the calibrated values are small except for α_2 and β_2 from table 1 and table 4. Even though $\Delta\alpha_2$ and $\Delta\beta_2$ are somewhat large, the coordinate values for the calibration points match well with the actual values as shown in Table 3 and the probe guide tool does not incline much as shown in Fig. 9, which means that the values of $\Delta\alpha_2$ and $\Delta\beta_2$ have a small influence on the position. The influence of $\Delta\alpha_2$ and $\Delta\beta_2$ on the position error, **e**, can be described as follows.

Table 4. Calibrated Kinematic Parameters of the Manipulator

Trans.	Type	θ	d	a	α
W→0	1	180.083°	0.083m	0.198m	89.2498°
0→1	2	-2.943°	0.993° (ß)	0.702m	0.2982°
1→2	2	-181.05°	-20.099° (ß)	0.833m	-25.862°
2→3	1	0°	-0.0184m	0m	0°

$$\mathbf{e} = \mathbf{T}_{3N}\begin{bmatrix} \cdots & 0 & z_3 & \cdots \\ \cdots & -z_3\cos\beta_2 & 0 & \cdots \\ \cdots & 0 & 0 & \cdots \\ O & 0 & 0 & O \end{bmatrix}\begin{bmatrix} \vdots \\ \Delta\alpha_2 \\ \Delta\beta_2 \\ \vdots \end{bmatrix}$$
$$= \mathbf{T}_{3N}\begin{bmatrix} \cdots & \cdots \\ \cdots & \cdots \\ \cdots & \cdots \\ O & O \end{bmatrix}\begin{bmatrix} \vdots \\ \vdots \end{bmatrix} + z_3\mathbf{T}_{3N}\begin{bmatrix} 0 & 1 \\ -\cos\beta_2 & 0 \\ 0 & 0 \\ 0 & 0 \end{bmatrix}\begin{bmatrix} \Delta\alpha_2 \\ \Delta\beta_2 \end{bmatrix}. \quad (16)$$

Here, z_3 is a linear displacement between the origins of the coordinate frames 2 and 3. Since the origin of the coordinate frame 2 is placed nearly on the tube sheet plane and all the calibration points are also on the tube sheet plane, the values of z_3 became small. Thus the values of $\Delta\alpha_2$ and $\Delta\beta_2$ have a small influence on the position, in other words, the values $\Delta\alpha_2$ and $\Delta\beta_2$ can become large even though the position errors are small.

4.2 Control Gain Tuning Response

Fig. 11 shows the experimental results of the PID control responses for the lower arm and the upper arm with the TDC-based gain tuning. The desired angle of the motor is 7,200 deg. Since an 810:1 ratio and a 408:1 ratio gear reducer are used for the shoulder joint and the elbow joint, respectively, the desired joint angles are 8.89 deg. and 17.6 deg. The results with a manual tuning are almost the same as shown in Fig. 11.

However, a difference in the control performance between the TDC-based gain tuning method and the manual gain tuning method can be found in Fig. 12. The solid line displays the results of the TDC-based gain tuning and the dotted line displays the results of the manual tuning. As shown in Fig. 12, the TDC-based gain tuning method provides a better performance for reducing not only the transient errors but also the vibrations causing noise. In addition, the PID gains can be determined easily because the TDC-based gain tuning method is systematic. It is noted that the magnitude of the transient errors is

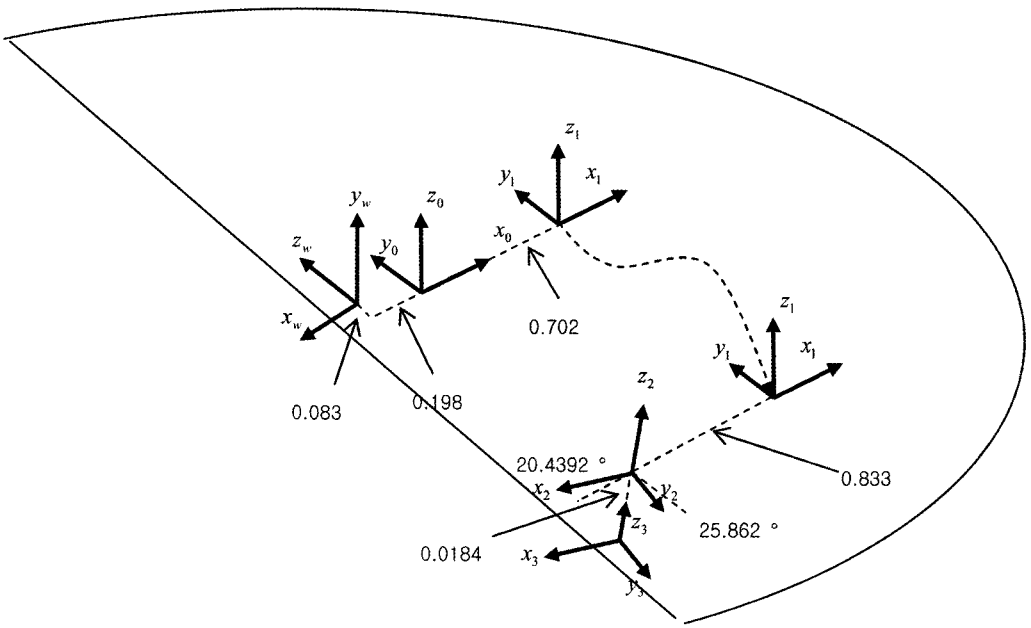

Fig. 10. Coordinate Frames after Calibration

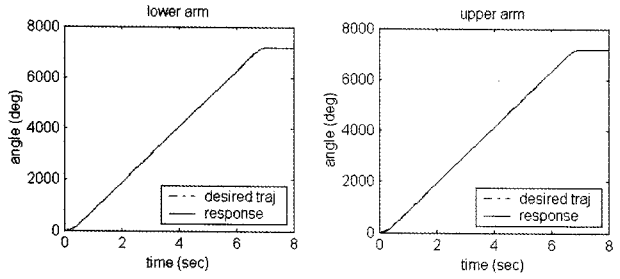

Fig. 11. Control Responses with a TDC-Based Gain Tuning

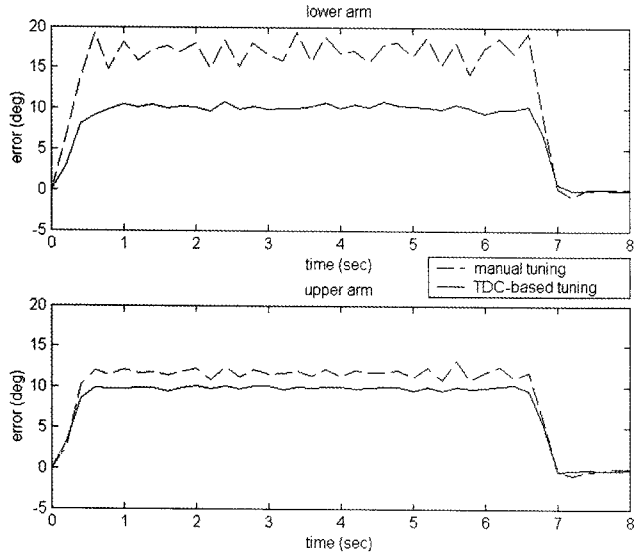

Fig. 12. Errors with the Manual Gain Tuning Method and the TDC-Based Gain Tuning Method

below 0.02 deg on the joint level and the magnitude of the regulating errors is below 10^{-4} deg.

4.3 Mockup Test

The final function test was carried out on the W F-Model type SG mockup located at the Kori NPP training center, which has 5,626 tubes with a pitch of 24.892 mm (0.98") [16]. Since the pitch between the tubes of the W F-Model type SG is smaller than that of the Framatome 51B Model type SG, the condition of the W F-Model type SG is more severe. However, the manipulator is calibrated and positioned on the target tube so that the ECT probe is inserted into the tubes accurately.

5. CONCLUSIONS

A nuclear steam generator tube inspection robotic system has been developed. For easy conveyance and installation, the robot was made of three separable parts: a manipulator base pose adjusting device, a water-chamber entering/exiting device, and a manipulator. It was designed to have a supporting leg which improves the rigidity of the system to increase the overall accuracy and to reduce the vibration level when the manipulator is moving. To improve the usability, a software program to control and manage the robotic system was developed on a Windows NT-based OS. The control program provides a real time 3-D graphic function that offers a remote reality. To insert the ECT probe into the SG tubes accurately, the manipulator was calibrated with the DH model and the modified DH model. Since there is no coordinate measuring machine in the SG chamber, the SG tubes were used for calibration points. Calibration point data were obtained through the CCD camera on the tool. The PID control gains were tuned systematically by the TDC-based tuning method. After calibration, the robot tool could be positioned on all tube holes without further calibration. Inspection works for SG tubes on the Framatome 51B Model type SG mockup and on the W F-Model type SG mockup were performed successfully by the developed robotic system.

ACKNOWLEDGMENT

This work was carried out under a nuclear R&D program by MOST (Ministry of Science and Technology) and MOCIE (Ministry of Commerce, Industry and Energy) in Korea.

REFERENCES

[1] EPRI NDE Center, *Advanced Eddy Current Data Analysis Techniques for Steam Generator Tubing*, 1984.

[2] P. Tipping, "Lifetime and Ageing Management of Nuclear Power Plants: A Brief Overview of Some Light Water Reactor component Ageing Degradation Problems and Ways of Mitigation", *Int. J. Pres. Ves. & Piping*, vol 66, pp. 17-25, 1996.

[3] S.W. Glass, J.B Fallon, C.F. Reinholtz and A.L. Abbott, "Machine Vision Calibration for a Nuclear Steam Generator Robot", *Robotics and Remote Systems*, pp. 512-513, 1994.

[4] S.J. Kang, J.C. Moon, D.H. Choi, S.S. Choi and H.G. Woo, "A distributed and intelligent system approach for the automatic inspection of steam-generator tubes in nuclear power plants", *IEEE Trans. on Nuclear Science*, vol. 45, Issue 3, pp. 1713 - 1722, June 1998.

[5] P. J. Hawkins and L. J. Petrosky, "Miniature manipulator for servicing the interior of nuclear steam generator tubes", *US patent US7,314,343 B2*, Jan., 2008.

[6] J. Miyafuchi, K. Tabuchi and T. Yamamoto, "Towards maintenance service supporting secure nuclear energy", *Mitsubishi Heavy Industries, Ltd. Technical Review*, vol. 40, no. 2, Apr., 2003.

[7] "ROSA III: the Westinghouse workhorse", *Nucl. Eng.* Int. vol. 36, no. 449, pp. 42-43, 1991.

[8] A. McLean et al., "Incremental Roadmaps and Global Path Planning in Evolving Industrial Environments," ICRA, pp.101~107, 1996.

[9] L. Obrutsky, J. Renaud and R. Lakhan, "Steam Generator

Inspections: Faster, Cheaper And Better, Are We There Yet?," *IV Pan American Conference for Non Destructive Testing 2007*, Buenos Aires, Argentina, Oct. 2007.

[10] B. Birgmajer, Z. Kovacic and Z. Postruzin, "Integrated Vision System for Supervision and Guidance of a Steam Generator Tube Inspection Manipulator," *IEEE Int. Conf. on Control Applications*, pp. 644~649, Munich, Germany, Oct. 2006.

[11] Z. Gan, L. T. Fitzgibbons, Q. Tang and J. S. Katz, "On-line robot work-cell calibration," *US patent 5,751,610*, May, 1998.

[12] B.W. Mooring, Z.S. Roth and M.R. Driels, *Fundamentals of Manipulator Calibration*, John Wiley & Sons, Inc., 1991.

[13] S. Hayati and M. Mirmirani. "A software for robot geometry parameter estimation", SME Paper #MS84-1052, presented at *Robots West Conference*, Anaheim, CA, November 1984.

[14] K. Youcef-Toumi and O. Ito, "A time delay controller for systems with unknown dynamics", *Trans. Of ASME, J. Dyn. Sys., Meas., Contr.*, vol. 112, no. 1, pp. 133-142, 1990.

[15] P.H. Chang, J.H. Jung and J. Lee, "A simple tuning method for robust MIMO PID control," in CDROM Proc. Int. Conf. Electrical Machines and Syst. (ICEMS), PD-11(630-S01-015) , 2004.

[16] The development of an inspection/maintenance robot for steam generator tubes, KAERI, KAERI/RR-2324/2002, 2002.